Spring 2-2012

Effects of Mismatched Electrodes on an AT-Cut Quartz Resonator

Huijing He
University of Nebraska-Lincoln, he.hui.jing@hotmail.com

Jinxi Liu
Shijiazhuang Tiedao University

Jiashi Yang
University of Nebraska-Lincoln, jyang1@unl.edu

Effects of Mismatched Electrodes on an AT-Cut Quartz Resonator

Huijing He, Jinxi Liu, and Jiashi Yang

***Abstract*—We study thickness-shear and thickness-twist free vibrations of a finite AT-cut quartz resonator with mismatched electrodes. The equations of anisotropic elasticity are used with the omission of the small elastic constant c_{56}. An analytical solution is obtained using Fourier series from which the resonant frequencies, mode shapes, and vibration confinement resulting from the electrode inertia are calculated and examined.**

I. Introduction

Electrodes are necessary parts of crystal resonators. They are used to electrically excite mechanical vibrations. The motional capacitance of a resonator is an important design consideration and is calculated from the charge (or current) and voltage on the electrodes. In plate thickness-shear (TSh) mode resonators, the electrode mass is responsible for energy trapping, through which the vibration is confined under the electrodes and decays rapidly outside them, a behavior crucial to resonator mounting. The electrode dimensions can be used to adjust the number of modes trapped under the electrodes [1], which lead to the important discovery of Bechmann's number, which defines the maximal dimensions for an electrode with only one trapped mode. In resonator manufacturing, one electrode is pre-deposited with a predetermined thickness. Then the electrode on the other side of the crystal plate has a thickness that is determined by the desired frequency of the electroded plate. This usually results in a crystal plate with two electrodes of different thicknesses. Electrodes of unequal thickness on the top and bottom of a plate resonator were studied in [2]–[5]. Recently, because of resonator miniaturization, the effects of electrode configurations have become an important design consideration. Electrodes of varying thickness have been shown to be effective in producing strong energy trapping [6]–[10], which provides a possible alternative to contoured resonators that are difficult to make. Electrode shape is another important factor. At present, circular and rectangular electrodes are still routinely used in manufacturing. In [11], it was recently shown that electrodes with corners cause field concentration and should be avoided in general. An important theoretical result on electrode shape and size was given by Mindlin [12], who obtained a formula for the optimal electrode shape and size of singly-rotated AT-cut quartz resonators using approximate two-dimensional plate equations. The electrodes determined in [12] satisfy Bechmann's number in every in-plane direction of an AT-cut quartz plate resonator. Based on the theoretical result of [12], numerical and graphical results were obtained in [13], showing that the commonly used rectangular and circular electrodes deviate significantly from the optimal electrodes, and therefore improvement in resonator performance may be expected using optimal electrodes. Optimal electrode shapes and sizes were also determined for doubly-rotated quartz resonators [14] and thin-film resonators [15].

An important and challenging issue in resonator design is that when the top and bottom electrodes on a plate resonator are mismatched, that is, when the centers of two identical electrodes shift away from the plate center (see Fig. 1 for an exaggerated and more general situation in which the two electrodes are not identical). There seem to be few theoretical results for this situation. In this paper, we study the effects of mismatched electrodes on the widely used TSh and thickness-twist (TT) modes in an AT-cut quartz plate resonator. The equations of anisotropic elasticity are used instead of the approximate plate equations. We examine the effect of mismatched electrodes on the resonant frequencies, mode shapes, and energy trapping.

II. Governing Equations

The equations for anisotropic crystals vary considerably according to crystal symmetry. The particular cut of a crystal plate refers to the orientation of the plate when it is taken out of a bulk crystal. As a consequence, crystal plates of different cuts exhibit different anisotropies in the plate coordinates normal and parallel to the plate surfaces. The widely used AT-cut quartz plate is a special case of rotated Y-cut quartz plates which are effectively monoclinic in the plate coordinate system. Consider such a plate, as shown in Fig. 1. The plate is unbounded in the x_1 direction and does not vary along x_1. Fig. 1 shows a cross section. The plate carries two different mass layers at the top and bottom surfaces. The mass layers are assumed to be very thin. Their inertia will be considered but their stiffness will be neglected. Quartz has very weak piezoelectric coupling. For free vibration frequency analysis, the small piezoelectric coupling can usually be neglected and an elastic analysis is sufficient. For monoclinic crystals, shear-horizontal or antiplane motions with only

Manuscript received August 25, 2011; accepted November 17, 2011.

H. He and J. Liu are with the Department of Engineering Mechanics, Shijiazhuang Tiedao University, Shijiazhuang, China.

H. He and J. Yang are with the Department of Mechanical and Materials Engineering, University of Nebraska–Lincoln, Lincoln, NE (e-mail: jyang1@unl.edu).

Digital Object Identifier 10.1109/TUFFC.2012.2188

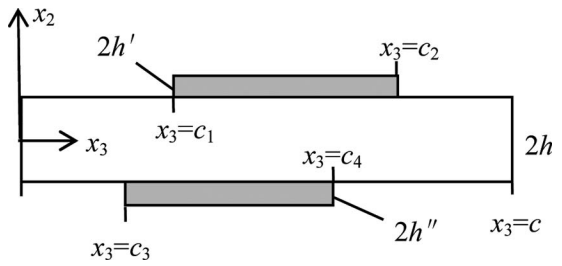

Fig. 1. A rotated Y-cut quartz plate with mismatched and unequal electrodes.

one displacement component are allowed by the linear theory of anisotropic elasticity. The corresponding modes are called TT modes in acoustic wave devices in general and include TSh and face-shear (FS) modes as special cases. Shear-horizontal motions in rotated Y-cut quartz are described by

$$u_1 = u_1(x_2, x_3, t), \quad u_2 = u_3 = 0, \tag{1}$$

where $\mathbf{u}$ is the displacement vector. The nonzero components of the strain tensor $\mathbf{S}$ and the stress tensors $\mathbf{T}$ are:

$$S_5 = 2S_{31} = u_{1,3}, \quad S_6 = 2S_{21} = u_{1,2}, \tag{2}$$

$$T_{31} = c_{55}u_{1,3} + c_{56}u_{1,2}, \quad T_{21} = c_{56}u_{1,3} + c_{66}u_{1,2}, \tag{3}$$

where $\mathbf{c}$ is the elastic stiffness tensor. The relevant equation of motion is

$$T_{21,2} + T_{31,3} = \rho\ddot{u}_1. \tag{4}$$

The equation to be satisfied by u_1 is obtained by substituting (3) into (4):

$$c_{66}u_{1,22} + c_{55}u_{1,33} + 2c_{56}u_{1,23} = \rho\ddot{u}_1. \tag{5}$$

For the plate in Fig. 1, the boundary condition at the plate's top surface is

$$T_{21} = \begin{cases} -2\rho' h'\ddot{u}_1, & x_2 = h, \quad c_1 < x_3 < c_2, \\ 0, & x_2 = h, \quad 0 < x_3 < c_1 \text{ or } c_2 < x_3 < c, \end{cases} \tag{6}$$

where ρ' and $2h'$ are the density and thickness of the mass layer. In $c_1 < x_3 < c_2$, the boundary condition in (6) represents Newton's second law applied to the mass layer. Similarly, the boundary condition at the plate bottom surface is

$$T_{21} = \begin{cases} 2\rho'' h''\ddot{u}_1, & x_2 = -h, \quad c_3 < x_3 < c_4, \\ 0, & x_2 = -h, \quad 0 < x_3 < c_3 \text{ or } c_4 < x_3 < c, \end{cases} \tag{7}$$

where the mass layer density and thickness are indicated by a double prime and may be different from those of the top layer. The boundary conditions at the left and right edges are

$$T_{31} = 0, \quad x_3 = 0, c, \quad |x_2| < h. \tag{8}$$

For AT-cut quartz plates, $c_{55} = 68.81$, $c_{56} = 2.53$, and $c_{66} = 29.01 \times 10^9$ N/m^2 [16]. c_{56} is very small compared with c_{55} and c_{66}. Therefore, in the rest of this paper, we will make the usual approximation of neglecting the small c_{56} [17].

III. Fourier Series Solution

Consider free vibrations. Let

$$u_1(x_2, x_3, t) = u_1(x_2, x_3)\exp(i\omega t). \tag{9}$$

We construct the following solution from separation of variables:

$$u_1 = A_0\cos(\eta_0 x_2) + B_0\sin(\eta_0 x_2) + \sum_{m=1}^{\infty}[A_m\cos(\eta_m x_2) + B_m\sin(\eta_m x_2)]\cos\frac{m\pi x_3}{c}, \tag{10}$$

where A_0, B_0, A_m, and B_m are undetermined constants, and

$$\eta_m^2 = \frac{\rho\omega^2}{c_{66}} - \frac{c_{55}}{c_{66}}\left(\frac{m\pi}{c}\right)^2 = \frac{\pi^2}{4h^2}\left[\frac{\omega^2}{\omega_s^2} - \frac{c_{55}}{c_{66}}\left(m\frac{2h}{c}\right)^2\right], \quad m = 0,1,2,3,\ldots, \tag{11}$$

$$\omega_s = \frac{\pi}{2h}\sqrt{\frac{c_{66}}{\rho}}. \tag{12}$$

Eq. (10) satisfies (5) and (8) when the small c_{56} is neglected. ω_s is the resonant frequency of the fundamental TSh mode in an unbounded quartz plate. Quartz resonators usually have large length/thickness ratios, i.e., $c \gg 2h$. In this case, for an m that is not large, η_m^2 is positive. We are interested in the first few TSh and TT modes with no more than a few nodal points along the x_3 direction, for which a large m is not needed. In the case when η_m^2 is nonpositive, the construction of the solution in (10) will be different. To apply the boundary conditions at the plate top and bottom, we need

$$T_{21} = c_{66}u_{1,2} = -c_{66}A_0\eta_0\sin(\eta_0 x_2) + c_{66}B_0\eta_0\cos(\eta_0 x_3) + c_{66}\sum_{m=1}^{\infty}[-A_m\eta_m\sin(\eta_m x_2) + B_m\eta_m\cos(\eta_m x_2)] \times \cos\frac{m\pi x_3}{c}. \tag{13}$$

Substitution of (10) and (13) into (6) and (7) gives (14) and (15), see next page. We multiply both sides of (14) by

$$-c_{66}A_0\eta_0\sin(\eta_0 h)+c_{66}B_0\eta_0\cos(\eta_0 h)+c_{66}\sum_{m=1}^{\infty}[-A_m\eta_m\sin(\eta_m h)+B_m\eta_m\cos(\eta_m h)]\cos\frac{m\pi x_3}{c}$$
$$=\begin{cases}2\rho' h'\omega^2\left\{A_0\cos(\eta_0 h)+B_0\sin(\eta_0 h)+\sum_{m=1}^{\infty}[A_m\cos(\eta_m h)+B_m\sin(\eta_m h)]\cos\frac{m\pi x_3}{c}\right\}, & c_1<x_3<c_2,\\ 0, & 0<x_3<c_1 \text{ or } c_2<x_3<c,\end{cases} \tag{14}$$

$$c_{66}A_0\eta_0\sin(\eta_0 h)+c_{66}B_0\eta_0\cos(\eta_0 h)+c_{66}\sum_{m=1}^{\infty}[A_m\eta_m\sin(\eta_m h)+B_m\eta_m\cos(\eta_m h)]\cos\frac{m\pi x_3}{c}$$
$$=\begin{cases}-2\rho'' h''\omega^2\left\{A_0\cos(\eta_0 h)-B_0\sin(\eta_0 h)+\sum_{m=1}^{\infty}[A_m\cos(\eta_m h)-B_m\sin(\eta_m h)]\cos\frac{m\pi x_3}{c}\right\}, & c_3<x_3<c_4,\\ 0, & 0<x_3<c_3 \text{ or } c_4<x_3<c.\end{cases} \tag{15}$$

$\cos(n\pi x_3/c)$ $(n=0,1,2,\dots)$ and integrate the resulting expression over $(0,c)$ to obtain

$$c_{66}\eta_0 c[-A_0\sin(\eta_0 h)+B_0\cos(\eta_0 h)]$$
$$=2\rho' h'\omega^2[A_0\cos(\eta_0 h)+B_0\sin(\eta_0 h)]C_{00}$$
$$+\sum_{m=1}^{\infty}[A_m\cos(\eta_m h)+B_m\sin(\eta_m h)]C_{nm},\quad n=0, \tag{16}$$

$$\frac{1}{2}cc_{66}[-A_n\eta_n\sin(\eta_n h)+B_n\eta_n\cos(\eta_n h)]$$
$$=2\rho' h'\omega^2\left\{[A_0\cos(\eta_0 h)+B_0\sin(\eta_0 h)]C_{0n}\right.$$
$$\left.+\sum_{m=1}^{\infty}[A_m\cos(\eta_m h)+B_m\sin(\eta_m h)]C_{mn}\right\}, \tag{17}$$
$$n=1,2,3,\dots,$$

where

$$C_{nm}=\int_{c_1}^{c_2}\cos\frac{n\pi x_3}{c}\cos\frac{m\pi x_3}{c}\,\mathrm{d}x_3$$
$$=\frac{1}{2}\left[\frac{c}{(n+m)\pi}\left(\sin\frac{(n+m)\pi c_2}{c}-\sin\frac{(n+m)\pi c_1}{c}\right)\right.$$
$$\left.+\frac{c}{(n-m)\pi}\left(\sin\frac{(n-m)\pi c_2}{c}-\sin\frac{(n-m)\pi c_1}{c}\right)\right]$$
$$=C_{mn},\quad m,n=0,1,2,\cdots,\quad m\neq n, \tag{18}$$

$$C_{00}=c_2-c_1,$$
$$C_{nn}=\frac{1}{2}\left[\frac{c}{2\pi n}\left(\sin\frac{2\pi n c_2}{c}-\sin\frac{2\pi n c_1}{c}\right)+c_2-c_1\right], \tag{19}$$
$$n=1,2,3,\dots.$$

Similarly, from (15) we can obtain

$$cc_{66}\eta_0[A_0\sin(\eta_0 h)+B_0\cos(\eta_0 h)]$$
$$=-2\rho'' h''\omega^2[A_0\cos(\eta_0 h)-B_0\sin(\eta_0 h)]D_{00}$$
$$-2\rho'' h''\omega^2\sum_{m=1}^{\infty}[A_m\cos(\eta_m h)-B_m\sin(\eta_m h)]D_{m0},\quad n=0, \tag{20}$$

$$\frac{1}{2}cc_{66}[A_n\eta_n\sin(\eta_n h)+B_n\eta_n\cos(\eta_n h)]$$
$$=-2\rho'' h''\omega^2\left\{[A_0\cos(\eta_0 h)-B_0\sin(\eta_0 h)]D_{0n}\right.$$
$$\left.+\sum_{m=1}^{\infty}[A_m\cos(\eta_m h)-B_m\sin(\eta_m h)]D_{mn}\right\},\quad n=1,2,3,\dots, \tag{21}$$

where D_{mn} is given by (18) and (19) with c_1 and c_2 replaced by c_3 and c_4. Eqs. (16), (17), (20), and (21) are linear homogeneous equations for A_0, B_0, A_m, and B_m. For nontrivial solutions, the determinant of the coefficient matrix must vanish, which determines the resonant frequencies. The nontrivial solutions of A_0, B_0, A_m, and B_m determine the corresponding modes. This is a complicated eigenvalue problem because the eigenvalue or the resonant frequency is present in every η_m. As nontrivial solutions to homogeneous equations, A_0, B_0, A_m, and B_m can be multiplied by an arbitrary constant. For the modes that we are interested in, B_0 is the major component; therefore, we will fix $B_0=1$, which effectively determines the arbitrary constant.

IV. Numerical Results

For quartz, $\rho=2649$ kg/m^3 [16]. We also introduce

$$\bar{\omega}_s=\omega_s(1-R),\quad R=\frac{\rho' h'+\rho'' h''}{\rho h}. \tag{22}$$

$\bar{\omega}_s$ is the resonant frequency of the fundamental thickness-shear mode in an unbounded quartz plate fully covered by

electrodes. R is the mass ratio between the electrodes and the plate. The resonant frequencies of the modes we are interested in are within $\bar{\omega}_s < \omega < \omega_s$. We consider a resonator with $c = 40$ mm and $2h = 1$ mm.

A. Identical Electrodes Without Mismatch

First, we consider the case of two identical electrodes without a mismatch as a reference. Both electrodes are 15 mm in length, located at the center with $c_1 = 12.5$ mm, $c_2 = 27.5$ mm, $c_3 = 12.5$ mm, and $c_4 = 27.5$ mm. We choose $R = 3\%$, which is larger than common electrodes to make their effects more obvious. In this case, there are three frequencies in the interval of $\bar{\omega}_s < \omega < \omega_s$. When using 17 ($n = 16$) and 18 ($n = 17$) terms in the series, the three frequencies are always found to be

$$\begin{aligned} &\omega_1/\omega_s = 0.974032, \quad \omega_2/\omega_s = 0.983082, \\ &\omega_3/\omega_s = 0.996098. \end{aligned} \tag{23}$$

Numerical tests show that A_0, B_0, A_n, and B_n are very sensitive to the frequencies. Six significant figures are used to ensure sufficient accuracy of the frequencies. In this case, the corresponding modes also converge very well, without noticeable differences. Therefore, all calculations below are based on 18 terms in the series. In this case, η_n^2 is positive. Twenty-seven ($n = 26$) or more terms will make η_n^2 negative.

The modes corresponding to the three frequencies are shown in Fig. 2, which is not drawn to scale. The first mode has no nodal points along the x_3 direction, which is the mode of interest and the one most useful in applications. It is a transversely varying TSh mode. The second and the third modes have one and two nodal points along the x_3 direction and are TT modes. For all of the modes in Fig. 2, the vibration is large in the central region and small near the plate edges at $x_3 = 0, c$. In other words, the vibration is mainly under the electrodes and decays outside them. This is the so-called energy trapping of TSh and TT modes.

We plot the plate top and bottom surface displacements of the first mode in Fig. 3(a). Their absolute values should be identical because the motion is antisymmetric about $x_2 = 0$. The difference of the absolute values of the two curves in Fig. 3(a) is shown in Fig. 3(b). The displacements in Fig. 3(a) are of the order of 1 and their difference in Fig. 3(b) is of the order of 10^{-8}, which should be treated as zero numerically.

B. Mismatched Electrodes

Consider the case when the two electrodes are identical (15 mm in length) but the top electrode is shifted to the right from the center by 2.5 mm and the bottom electrode is shifted to the left by 2.5 mm. In this case $c_1 = 15$ mm, $c_2 = 30$ mm, $c_3 = 10$ mm, and $c_4 = 25$ mm. We still use $R = 3\%$. In this case, the following three frequencies are found:

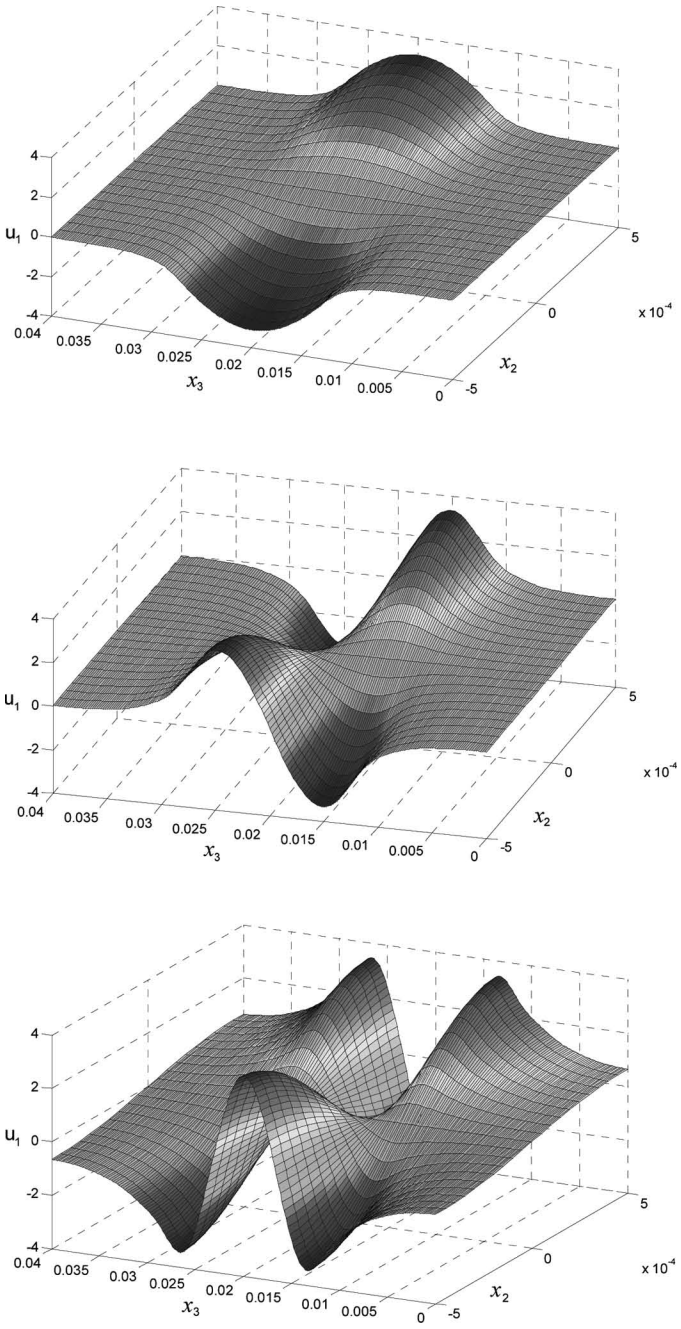

Fig. 2. Identical electrodes without mismatch: three trapped modes.

$$\begin{aligned} &\omega_1/\omega_s = 0.975396, \quad \omega_2/\omega_s = 0.986455, \\ &\omega_3/\omega_s = 0.996121, \end{aligned} \tag{24}$$

which are higher than those in (23). For the first frequency, the difference between (24) and (23) is 0.001364, which is significant in resonator applications, for which relative frequency shifts are measured in parts per million. The three modes still look like those in Fig. 2. For a closer look, we plot the plate top and bottom surface displacements of the first mode in Fig. 4(a); they look identical, as in Fig. 3(a), but the difference of their absolute values shown in Fig. 4(b) is of the order of 0.01, much larger than that in Fig. 3(b) and cannot be treated as zero numeri-

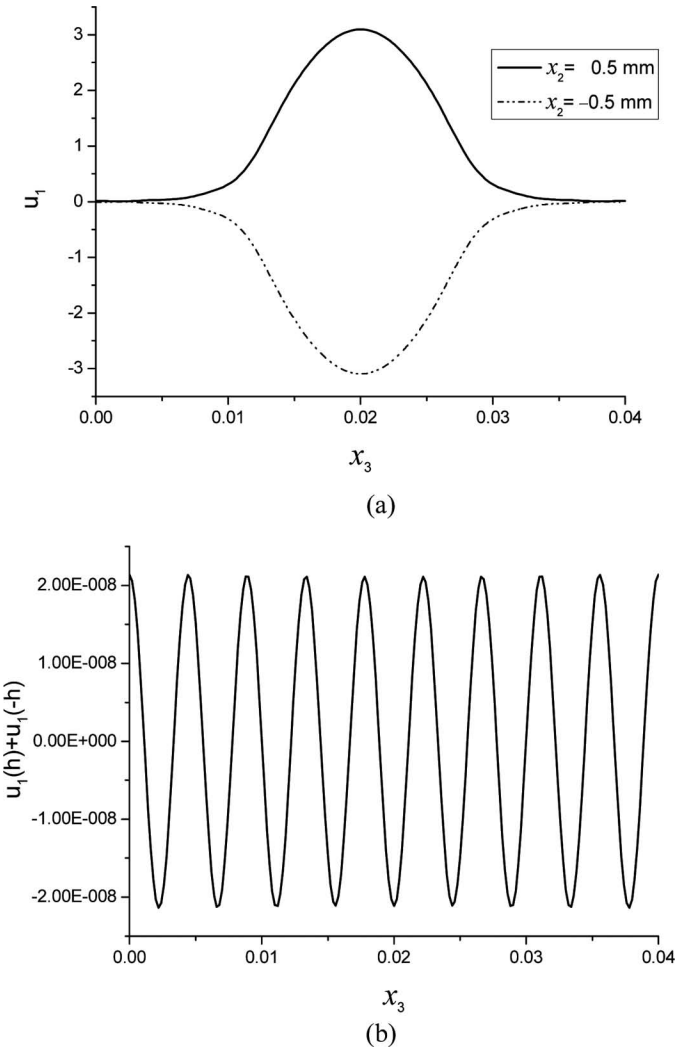

Fig. 3. Identical electrodes without mismatch: (a) plate top and bottom surface displacements. (b) Difference of the absolute values of the plate top and bottom surface displacements.

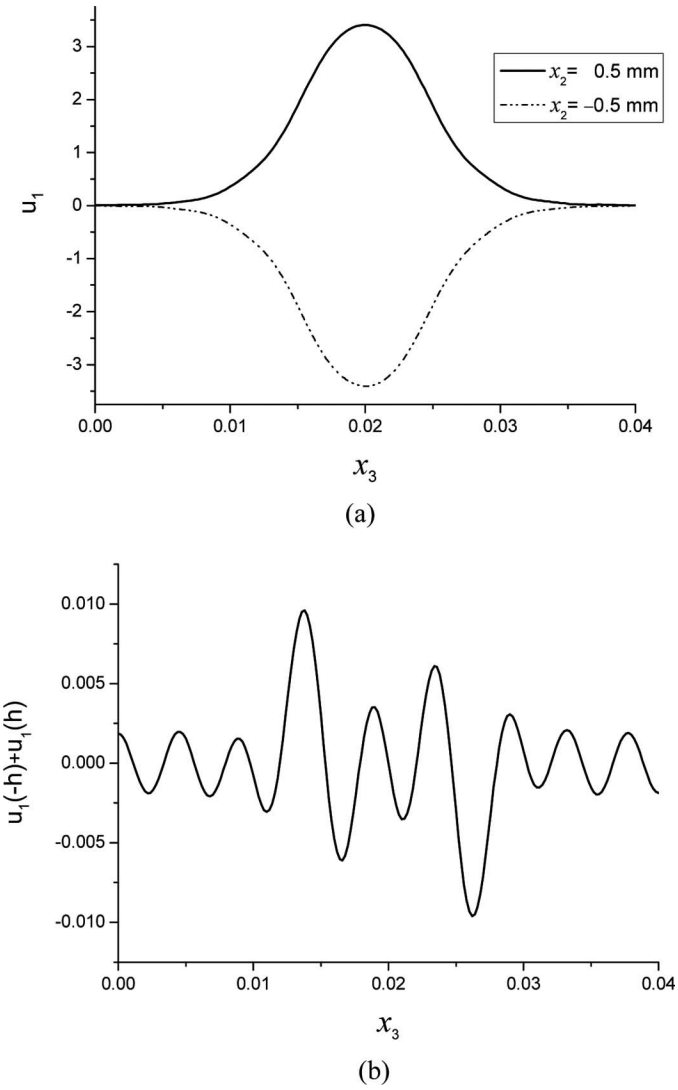

Fig. 4. Mismatched electrodes of the same length: (a) plate top and bottom surface displacements. (b) Difference of the absolute values of the plate top and bottom surface displacements.

cally. In addition, Fig. 4(b) is antisymmetric about $x_3 = c/2$, which is consistent with the fact that the top and bottom electrodes have shifted in opposite directions and introduced some antisymmetry in the structure.

C. Electrodes of Unequal Length

Electrodes with different lengths are also of concern in design and the effects are little known. Consider the case in which the top electrode is 10 mm long and the bottom electrode is 20 mm long. The total length of the two electrodes is 30 mm, the same as the two previous cases. Both electrodes are at the centers of the plate surfaces. In this case $c_1 = 15$ mm, $c_2 = 25$ mm, $c_3 = 10$ mm, and $c_4 = 30$ mm. For the same $R = 3\%$, the three resonant frequencies are found to be exactly the same as those in (24). The top and bottom surface displacements and the difference of their absolute values are shown in Figs. 5(a) and 5(b), respectively. The magnitude of the displacement difference is of the order of 0.01, and it is symmetric about $x_3 = c/2$, as expected.

D. Comparison

In Fig. 6, we compare the plate top surface displacement of the first mode for the three electrode configurations considered here. The case of mismatched electrodes and the case of electrodes with unequal length are indistinguishable. It can be seen that the displacement is more confined to the center when the electrodes are mismatched or with unequal length. It seems that for mismatched electrodes, energy trapping is mainly dependent on the overlapped region of the electrodes, which is shorter than the electrode length; for electrodes of unequal length, energy trapping mainly depends on the shorter electrode. The fact that the vibration is more confined for mismatched or unequal electrodes is consistent with the slightly higher frequencies in these two cases.

V. Conclusion

A Fourier series solution was obtained for TSh and TT vibrations of an AT-cut quartz resonator with a pair of

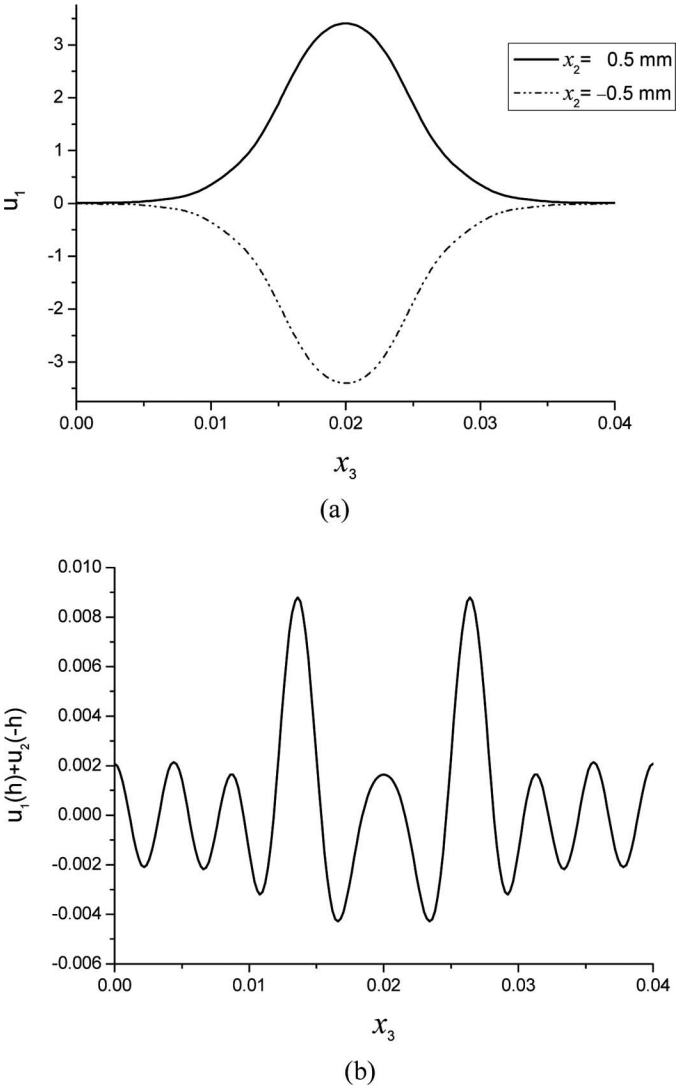

Fig. 5. Unequal electrodes without mismatch: (a) plate top and bottom surface displacements. (b) Difference of the absolute values of the plate top and bottom surface displacements.

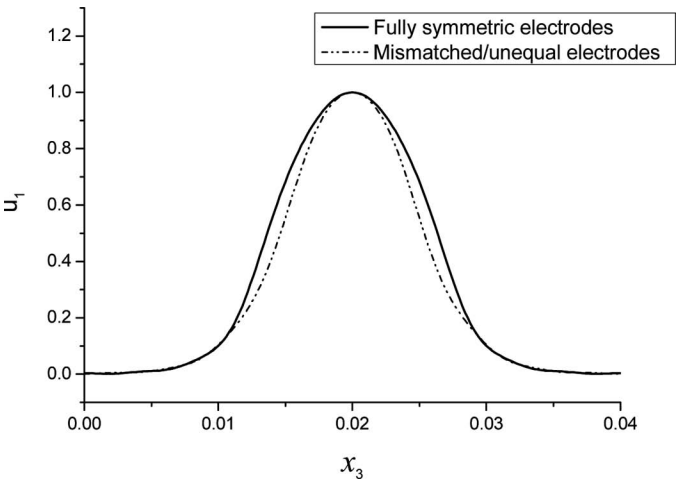

Fig. 6. Comparison of the plate top displacements of the first mode in different cases.

arbitrary electrodes. Numerical results calculated from the solution show that mismatched electrodes raise the resonant frequencies in the order of 0.001 for relative frequency shifts and make a difference in the plate top and bottom surface displacements in the order of 0.01. Electrodes of unequal length have similar effects. For mismatched electrodes, energy trapping is mainly dependent on the overlapped region of the electrodes; for electrodes of unequal length, energy trapping mainly depends on the shorter electrode.

References

[1] R. D. Mindlin and P. C. Y. Lee, "Thickness-shear and flexural vibrations of partially plated, crystal plates," *Int. J. Solids Struct.*, vol. 2, no. 1, pp. 125–139, 1966.

[2] F. Boersma and E. C. van Ballegooyen, "Rotated Y-cut quartz crystal with two different electrodes treated as a one-dimensional acoustic composite resonator," *J. Acoust. Soc. Am.*, vol. 62, no. 2, pp. 335–340, 1977.

[3] J. A. Kosinski, "Thickness vibrations of flat piezoelectric plates with massy electrodes of unequal thickness," in *Proc. IEEE Ultrason. Symp.*, 2003, pp. 70–73.

[4] J. Wang and L. J. Shen, "Exact thickness-shear resonance frequency of electroded piezoelectric crystal plates," *J. Zhejiang Univ. Sci.*, vol. 6A, no. 9, pp. 980–985, 2005.

[5] J. S. Yang, H. G. Zhou, and W. P. Zhang, "Thickness-shear vibration of rotated Y-cut quartz plates with relatively thick electrodes of unequal thickness," *IEEE Trans. Ultrason. Ferroelectr. Freq. Control*, vol. 52, no. 5, pp. 918–922, 2005.

[6] S. Y. Pao, R. Huang, and C. S. Lam, "Energy trapping effect of stepped electrode in miniature AT-cut quartz resonator," in *Piezoelectricity, Acoustics Waves and Device Applications*. Singapore: World Scientific, 2007, pp. 152–154.

[7] J. S. Yang, H. Xue, H. Y. Fang, Y. T. Hu, J. Wang, and L. J. Shen, "Effects of electrodes with varying thickness on energy trapping in thickness-shear quartz resonators," *IEEE Trans. Ultrason. Ferroelectr. Freq. Control*, vol. 54, no. 4, pp. 892–895, 2007.

[8] J. Wang, L. J. Shen, and J. S. Yang, "Effects of electrodes with continuously varying thickness on energy trapping in thickness-shear mode quartz resonators," *Ultrasonics*, vol. 48, no. 2, pp. 150–154, 2008.

[9] J. S. Yang, Z. G. Chen, and H. P. Hu, "Electrically forced vibration of a thickness-twist mode piezoelectric resonator with non-uniform electrodes," *Acta Mech. Solida Sin.*, vol. 20, no. 4, pp. 266–274, 2007.

[10] J. S. Yang, Z. G. Chen, and Y. T. Hu, "Vibration of a thickness-twist mode piezoelectric resonator with asymmetric, non-uniform electrodes," *IEEE Trans. Ultrason. Ferroelectr. Freq. Control*, vol. 55, no. 4, pp. 841–848, 2008.

[11] J. S. Yang, H. Xue, and Y. T. Hu, "Finite element analysis of stress field concentration near the edge of an electrode," *Ferroelectr. Lett. Sect.*, vol. 34, no. 3–4, pp. 108–112, 2007.

[12] R. D. Mindlin, "Optimal sizes and shapes of electrodes for quartz resonators," *J. Acoust. Soc. Am.*, vol. 43, no. 6, pp. 1329–1331, 1968.

[13] Z. T. Yang and J. S. Yang, "Optimal electrode shape and size of a few singly rotated quartz and langasite resonators," *IEEE Trans. Ultrason. Ferroelectr. Freq. Control*, vol. 56, no. 2, pp. 237–238, 2009.

[14] Z. T. Yang, J. S. Yang, and Y. T. Hu, "Optimal electrode shape and size of doubly rotated quartz plate thickness mode piezoelectric resonators," *Appl. Phys. Lett.*, vol. 92, no. 10, art. no. 103516, 2008.

[15] L. M. Xu, B. B. Tang, Y. T. Hu, H. Fan, and J. S. Yang, "Optimal electrode shape and size for shear mode thin film acoustic wave resonators," *Appl. Phys. Lett.*, vol. 95, no. 23, art. no. 233501, 2009.

[16] H. F. Tiersten, *Linear Piezoelectric Plate Vibrations*. New York, NY: Plenum, 1969.

[17] H. F. Tiersten, "Analysis of trapped-energy resonators operating in overtones of coupled thickness shear and thickness twist," *J. Acoust. Soc. Am.*, vol. 59, no. 4, pp. 879–888, 1976.

Authors' photographs and biographies were unavailable at time of publication.